# Properties of terahertz wave generated by the metallic carbon nanotube antenna

**Yue Wang (王 玥)[1,2] and Qun Wu (吴 群)[1]**

[1]*School of Electronics and Information Technology, Harbin Institute of Technology, Harbin 150001*

[2]*Department of Electrical Science and Technology, Harbin University of Science and Technology, Harbin 150080*

Received July 16, 2008

The properties of terahertz (THz) radiation pulses emitted by a metallic, large aspect ratio carbon nanotube antenna have been studied both in the THz waveforms and field distribution. The peak THz field up to 2.66 and 1.26 kV/cm are observed at the probe points. The proposed antenna is designed to operate for dual frequency applications from 2.36 to 2.58 THz and from 7.27 to 7.5 THz for less than −10 dB return loss.

*OCIS codes:* 320.7120, 320.5390, 350.5610, 350.4238.

*doi: 10.3788/COL20080610.0770.*

Carbon nanotubes (CNTs) have been attracting much attention of scientists and engineers because of their unique physical, topological, and mechanical properties. Especially, the outstanding electronic properties of CNTs offer the possibilities of using them in diverse applications ranging from nanoelectronics devices to chemical and biochemical sensors[1−5]. Single-walled carbon nanotubes (SWCNs) can be regarded as a seamless cylinder consisting of a sheet of graphite rolled up into a tube having a radius of a few nanometers and a length up to centimeters, and then multi-walled carbon nanotubes (MWCNs) are made by SWCNs nested concentrically inside one another. Experiments and theories have shown that CNTs can be either metallic with excellent conductivity or semiconducting with a band gap inversely proportional to the diameter of the tube, depending on their different chirality.

Based on the outstanding metallic and quasi-one-dimensional ballistic transportation of electron of CNTs, the visible and infrared antenna for CNTs has been studied both experimentally and theoretically. The first studies on the visible antenna effects of CNTs were in 2004, where the polarization effect and the antenna effect have been demonstrated. And the characteristics of armchair CNTs have been actively discussed in infrared and optical regime[6−10]. However, their terahertz (THz) radiation properties have not been investigated thoroughly[11]. To complete the preliminary THz wave antenna studies, it is useful to performe computer simulations of the detailed antenna radiation properties in the THz range. In this letter, the THz electromagnetic radiation properties of CNTs antenna are studied based on the computer simulation technology (CST).

As in graphite, the bonding in CNTs is $sp^2$ with each atom joined to three neighbors. The tubes can therefore be considered as rolled up grapheme sheets. The structure of CNTs can be specified by vector $\vec{C}_{\rm h} = n\vec{a}_1 + m\vec{a}_2$, where $n$, $m$ are integers and $\vec{a}_1$, $\vec{a}_2$ are lattice basis vectors. Thus CNTs can be characterized by the dual index $n$, $m$. The first two types, known as armchair ($n = m$) and zigzag ($n = 0$) carbon nanotubes have a high degree of symmetry. The third type is chiral carbon nanotube ($m \neq n > 0$) which is most commonly used in practice. Armchair CNTs are always metallic, therefore attention will be focused on armchair SWCNs. The radius of CNTs is given by

$$R = \frac{C_{\rm h}}{2\pi} = \frac{\sqrt{3}}{2\pi} a_{\rm c-c} \sqrt{n^2 + nm + m^2}, \tag{1}$$

where $a_{\rm c-c} = 0.142$ nm is the interatomic distance in grapheme. Figure 1 shows the construction of the CNT antenna and its corresponding coordinates. The radius and total length of the antenna are $R$ and $L$, respectively, and the gap between dipole is $d$ ($d \ll L$). Theoretically, a simple dipole thin antenna maximizes its response to a wavelength $\lambda$ in condition of $L = m\lambda/2$, where $m$ is a positive integer.

Figure 2(a) shows a typical transient THz electric field waveform observed in the direction parallel to the dipole antenna at $r = (5, 0, 0)$ $\mu$m, although no dipole field is expected in this direction within the common hertzian approach. The first main positive and negative peaks of pulse have full-width at half-maxima (FWHM) of 59 and 56 fs, respectively. One can note that THz pulse has a delay of about 164 fs and the THz signal shows several peaks corresponding to multiple THz reflections in the antenna. The maximum peak of THz field is up to 2.66 kV/cm. Figure 2(b) shows a transient far field THz pulse in the direction at $r = (10, 0, 0)$ $\mu$m. We note that there is a delay of approximately 181 fs because of the propagation from the antenna edges to a probing point in the far field. The initial negative peak with a width of 56 fs is followed by a high peak pulse which persists for about 0.16 ps. As depicted in Fig. 2(b), the maximum peak of THz field decreases to 1.26 kV/cm in comparison

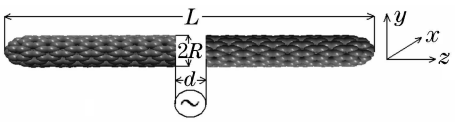


Fig. 1. Structure of CNT (armchair) antenna.

 

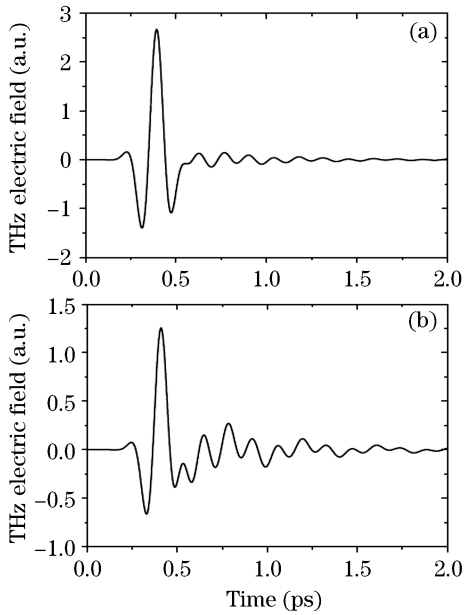


Fig. 2. THz pulse in the direction parallel to the dipole antenna (a) $r = (5, 0, 0)$ $\mu$m; (b) $r = (10, 0, 0)$ $\mu$m.

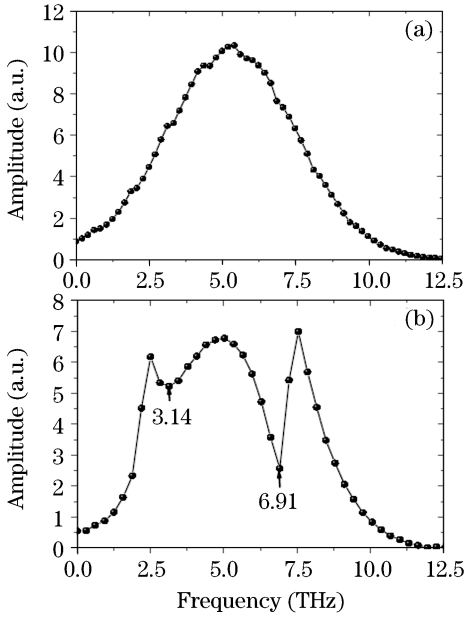


Fig. 3. Fourier amplitude of the waveforms shown in Fig. 2. (a) The corresponding frequency distributions calculated for the THz pulse in Fig. 2(a) and (b) the corresponding frequency distributions calculated for the THz pulse in Fig. 2(b).

with that of Fig. 2(a). Some weaker oscillations can be obviously seen for longer delays and the average oscillation period of THz pulse is roughly 0.13 ps, which can be resulted from current multiple reflections in the CNT antenna.

Figure 3 shows Fourier transformed amplitude spectrum of the THz wave forms shown in Fig. 2. From the figures, it can be seen that the spectrum profiles are different between the two cases. The spectra of THz pulses peaks are roughly at 5.3 and 5.0 THz shown in Figs. 3(a) and (b), respectively. The spectral dips at 3.14 and 6.91 THz are observed in Fig. 3(b). The high frequency of spectral distribution extends about 12.5 THz, which are less than 30 THz reported so far for the photoconductor antenna. But such results imply another approach to generate a THz source by the CNTs antenna.

The scattering parameter (S11) and voltage standing wave ratio (VSWR) as a function of frequency are shown in Fig. 4, where the first resonant frequency (2.47 THz) is approximately equal to 2.5 THz by the practical electrical length calculated when the S11 $< -10$ dB and the second resonant frequency is 7.38 THz. VSWR is less than 1.5:1 on the operating frequency from 2.36 to 2.58 THz and from 7.27 to 7.5 THz, corresponding to S11 $< -10$ dB bandwidths of 8.9% and 3.1%.

To highlight the THz radiation electric field production of CNTs, we use finite integration method to calculate spatial electric field distribution in different directions at resonant frequencies of 2.47 and 7.38 THz shown pictorially in Fig. 5. As expected, strong THz fields are created within the antenna. Figures 5(a) and (b), (c) and (d), (e) and (f) correspond to the planes $z = 30$ $\mu$m, $x = 30$ $\mu$m, and $y = 7$ $\mu$m, respectively. As can be recognized, there is a strong confinement effect on the surface of CNTs which becomes increasingly more pronounced for high frequencies. We note that although the THz field distributions are different, they are symmetric in all three

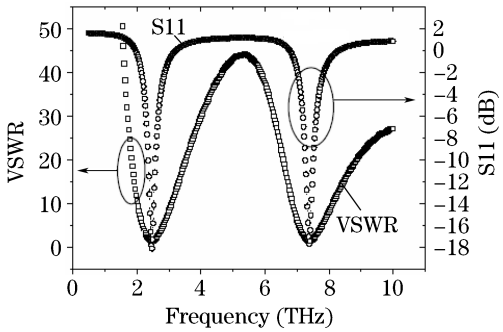


Fig. 4. Scattering parameter and voltage standing wave ratio of antenna.

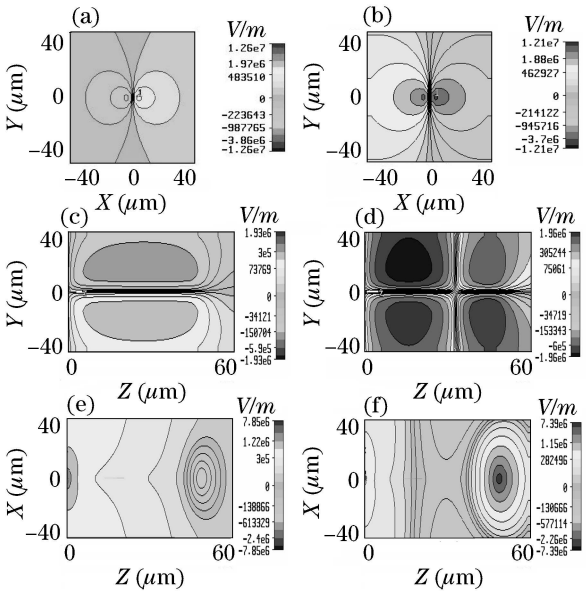


Fig. 5. THz electric field distribution at various spatial planes. (a), (c), (e) and (b), (d), (f) are for the frequencies of 2.47 THz and 7.38 THz, respectively.

directions. As shown in Fig. 5, the THz electric intensity in higher frequency is stronger than that in low frequency and the period distributions of electric field are obtained in high frequency in Fig. 5(e). The spatial patterns on the $x$-$z$ planes differ for various frequencies: the 2.47 THz frequency component propagates to the end of CNTs in the $z$ direction with a continuously attenuation, while the 7.38 THz component first decreases to zero, and then increases along the $z$ direction. This suggests that the high frequency components of THz radiation are more easily generating oscillation.

In summary, we have investigated the properties of THz emission from metallic, dipole SWCN antenna by CST simulation tool. Our calculation elucidates the features of field patterns of the THz are transient in different frequencies. Besides the THz field transients, the radiation patterns of the resonant frequencies are observed. A direct comparison is made with the THz emission field properties of CNT antenna in different resonant frequencies. The simulation technique provides a powerful tool to study the detailed features of THz electric transients on the CNTs antenna and in the far-field space. These results can be used in the design of optimal emitters to generate high-energy THz pulse trains for applications in communications, nonlinear optics, and coherent control.

This work was supported by the National Natural Science Foundation of China (No. 60571026). Y. Wang's e-mail address is wsbte@126.com.

## References

1. S. Heinze, J. Tersoff, and R. Martel, Phys. Rev. Lett. **89,** 106801 (2002).
2. J. Appenzeller, J. Knoch, and V. Derycke, Phys. Rev. Lett. **89,** 126801 (2002).
3. J. Wang and M. Musameh, Analyst. **129,** 1 (2004).
4. Y. J. Sun, Y. Cheng, F. Wang, and J. M. Li, Chin. Phys. Lett. **21,** 447 (2004).
5. B. D. Huang, Y. Y. Xia, and M. W. Zhao, Chin. Phys. Lett. **21,** 2388 (2004).
6. M. S. Dresselhaus, Nature **432,** 959 (2004).
7. P. J. Burke, S. Li, and Z. Yu, IEEE Trans. Nanotechnol. **5,** 314 (2006).
8. H. Jin and G. W. Hanson, IEEE Trans. Nanotechnol. **5,** 766 (2006).
9. K. Kempa, J. Rybczynski, and Z. P. Huang, Advanced Materials **19,** 421 (2007).
10. Y. Wang, K. Kempa, and B. Kimball, Appl. Phys. Lett. **85,** 2607 (2004).
11. Y. Wang, Q. Wu, and W. Shi, International Journal of Infrared and Millimeter Waves **29,** 35 (2008).